Numerical aspects of Casimir energy computation in acoustic and electromagnetic scattering

Timo Betcke[a], Alexander Strohmaier[b], Xiaoshu Sun[a,*]

[a]*Department of Mathematics, University College London, London, WC1E 6BT, UK*
[b]*School of Mathematics, University of Leeds, Leeds, LS2 9JT, UK*

Abstract

Computing the Casimir energy is a classical problem of quantum electrodynamics going back to the 1940s. In the early two thousands a significant breakthrough was achieved by representing the Casimir energy as the computation of the integral of the log determinant of certain boundary integral operators in the complex plane. Recently, this log determinant formula was investigated in the context of the Krein spectral shift function, which suggests a potential alternative computational approach based on the numerical evaluation of scattering matrices. In this paper, we will give an overview of these computational techniques of computing the Casimir energy in three dimensional acoustic and electromagnetic scattering. Afterwards, we will discuss the spectral properties of the block matrices inside the formula of the Casimir energy, which are constructed by the integral operators and investigate how to use these properties to speed up Casimir computations for large-scale practical problems.

Keywords: Krein spectral shift function, Casimir energy, Krylov subspace, inverse-free generalized eigenvalue problem, Bempp

---

1. Introduction

Since late 1940s, the advanced understanding of vacuum sector of quantum electrodynamics has been developed and one of the most seminal predictions is the vacuum effects (quantum fluctuations of the electromagnetic field) can induce attractive forces between two uncharged, perfectly conducting, parallel plates. This phenomenon is called *Casimir effect*, which is firstly proposed by H.B.G. Casimir in 1940s [1]. To obtain the formula of the Casimir energy, he considered the space between these two plates as a type of electromagnetic cavity, solved the classical Maxwell equations with certain boundary condition for all the valid excitations of the electromagnetic field in this cavity and obtained countably infinite electromagnetic mode frequencies $\{\omega_n(a)\}$, where a is the surface-surface distance. Accordingly, the electromagnetic zero-point energy of the nth cavity mode is $\frac{\hbar\omega_n(a)}{2}$ and by summing up all the contributions from the modes, he finally get the expression of the *Casimir energy*:

$$\mathcal{E}(a) = \frac{1}{2}\sum_n \hbar\omega_n(a),$$

which is divergent. However, Casimir derived a finite result for the derivative of this infinite energy fluctuations, which is the *Casimir force per unit area*:

$$F(a) = -\frac{1}{A}\frac{\partial\mathcal{E}}{\partial a} = -\frac{\hbar c\pi^2}{240a^4},$$

where A is the cross-sectional area of the boundary plates.

---

*Corresponding author
URL:* t.betcke@ucl.ac.uk (Timo Betcke), a.strohmaier@leeds.ac.uk (Alexander Strohmaier), xiaoshu.sun.18@ucl.ac.uk (Xiaoshu Sun)

In 1960s, Lifshitz generalized this theory to the case of dielectric media [2], which means the boundary surfaces are not perfect conductors but the real-world materials such us the solid consisting of the atomic constituents. He proposed that any microscopic volume ΔV of the plates contains a collection of atomic-scale electric dipoles without uniform orientation due to the absence of the external forcing field. Once in a while, the quantum and thermal fluctuations may make the dipoles align spontaneously, resulting in a net electric dipole moment. It is like van der Waals interaction between the atoms and this dipole moment induces a net dipole field. Meanwhile, the dipoles in the opposite plate feel this field across the gap and align as well. Now, there are two net electric dipole moments which make two plates attract with each other. Lifshitz emphasized the influence from the materials more than the fluctuations in the empty space between the plates and this interpretation provides little advantage on the computation of the Casimir energy since it is unknown on how to compute each contribution from the volume ΔV.

Afterwards, there is a decades absence of experimental input on the Casimir effect and finally in 1996, the precise measurements of the Casimir force between the extended bodies have been done by S.K. Lamoreaux [3]. From 2000 to 2008, the Casimir force has been measured in various experimental configurations, such as cylinder-cylinder [4], plate-plate [5], sphere-plate [6] and sphere-comb [7]. The rapid growth in experimental investigation is followed by the theoretical development. From 2007 to 2008, the asymptotic series of the Casimir energy have been explicitly computed by T. Emig's team in both scalar [8] and vector [9] cases. In 2009, Johnson's team put forward a method of computing the Casimir interactions between arbitrary three-dimensional objects with arbitrary material properties [10], in which the Casimir energy between the perfectly conducting compact objects can be described as:

$$\mathcal{E} = -\frac{\hbar c}{2\pi} \int_0^\infty dk \log \frac{\mathcal{Z}(k)}{\mathcal{Z}_\infty(k)},$$

where

$$\mathcal{Z}(k) = \int \mathcal{D}\boldsymbol{J}(\boldsymbol{x}) e^{\frac{1}{2} \int \int d\boldsymbol{x} d\boldsymbol{y} \boldsymbol{J}(\boldsymbol{x}) \cdot \boldsymbol{G}_k(\boldsymbol{x}, \boldsymbol{y}) \cdot \boldsymbol{J}(\boldsymbol{y})} \tag{1}$$

is a functional integration extending over all possible surface current distributions $\boldsymbol{J}(\boldsymbol{x})$ on the objects and $\mathcal{Z}_\infty(k)$ is $\mathcal{Z}(k)$ computed with all the objects removed to infinite separation. Moreover, in (1),

$$\boldsymbol{G}_k(\boldsymbol{x}, \boldsymbol{y}) = \left[1 + \frac{1}{k^2} \nabla_{\boldsymbol{x}} \otimes \nabla_{\boldsymbol{y}} \right] \frac{e^{ik|\boldsymbol{x}-\boldsymbol{y}|}}{4\pi|\boldsymbol{x}-\boldsymbol{y}|}$$

is the dyadic/tensor Green's function and k is the wavenumber. Johnson proposed that one could formally apply contour integral arguments to obtain the integral along the imaginary axis on which the integrand is nicely behaved (non-oscillatory and exponentially decaying). In this case, the Casimir energy formula is rewritten as

$$\mathcal{E} = -\frac{\hbar c}{2\pi} \int_0^\infty dk \log \frac{\mathcal{Z}(ik)}{\mathcal{Z}_\infty(ik)}, \tag{2}$$

where

$$\mathcal{Z}(ik) = \int \mathcal{D}\boldsymbol{J}(\boldsymbol{x}) e^{\frac{1}{2} \int \int d\boldsymbol{x} d\boldsymbol{y} \boldsymbol{J}(\boldsymbol{x}) \cdot \boldsymbol{G}_{ik}(\boldsymbol{x}, \boldsymbol{y}) \cdot \boldsymbol{J}(\boldsymbol{y})} \tag{3}$$

and

$$\boldsymbol{G}_{ik}(\boldsymbol{x}, \boldsymbol{y}) = \left[1 - \frac{1}{k^2} \nabla_{\boldsymbol{x}} \otimes \nabla_{\boldsymbol{y}} \right] \frac{e^{-k|\boldsymbol{x}-\boldsymbol{y}|}}{4\pi|\boldsymbol{x}-\boldsymbol{y}|}.$$

This $\boldsymbol{G}_{ik}$ is called the Wick-rotated dyadic/tensor Green's function. One can notice that this Green's function is strongly singular due to the second order form ($\nabla_{\boldsymbol{x}} \otimes \nabla_{\boldsymbol{y}}$).

However, a more rigorous mathematical derivation was recently provided by Hanisch, Strohmaier and Waters [11] who have shown that the natural and well-defined object is the integral along the imaginary axis. They also provided a mathematical framework to connect the integral to families of trace formulas and the Casimir energy is one of the examples. To be specific, by assuming that the objects Ω is assembled from individual objects Ω_j, for $j = 1, \ldots, N$ and $\partial\Omega_j$ are the N connected components of the boundary $\partial\Omega$. Then, several self-adjoint operators on $L^2(\mathbb{R}^d)$ can be defined for constructing the *Birman-Krein formula* later:

- The operator Δ is the Laplace operator with Dirichlet boundary conditions on $\partial\Omega$.

- For $j = 1, \ldots, N$, the operator Δ_j is the Laplace operator with Dirichlet boundary conditions on $\partial\Omega_j$.

- The operator Δ_0 is the 'free' Laplace operator on $\mathbb{R}^d$ with domain $H^2(\mathbb{R}^d)$.

Now, the Birman-Krein formula can be written as

$$\text{Tr}\left(f(\Delta^{\frac{1}{2}}) - f(\Delta_0^{\frac{1}{2}}) - \left(\sum_{j=1}^{N}[f(\Delta_j^{\frac{1}{2}}) - f(\Delta_0^{\frac{1}{2}})]\right)\right) = \int_0^\infty f'(k)\xi(k)dk, \tag{4}$$

where

$$\xi(k) = \frac{1}{2\pi i}\log\left(\frac{\det(S(k))}{\det(S_{1,k})\cdots\det(S_{N,k})}\right)$$

is called the *Krein spectral shift function*. Here, $\det(S_{j,k})$ are the scattering matrices of Δ_j associated to the objects Ω_j.

According to [11], by setting $f(x) = x$, (4) becomes

$$\text{Tr}\left(\Delta^{\frac{1}{2}} + (N-1)\Delta_0^{\frac{1}{2}} - \sum_{j=1}^{N}\Delta_j^{\frac{1}{2}}\right) = \int_0^\infty \xi(k)dk.$$

This formula can be used to compute the Casimir energy and it can be an alternative efficient method based on the numerical evaluation of scattering matrices whose dimension depends on the number of the spherical harmonic functions used in the spherical expansion of the incident/scattering waves.

In this paper, we are going to introduce the numerical framework of computing the Casimir energy based on the evaluation of the log determinant of the integral operators in both acoustic and electromagnetic cases in Section 2 and discuss the spectral properties of the block matrices constructed from the integral operators in Section 3. Afterwards, with these properties, an inverse-free method of computing the integrand of the Casimir energy will be illustrated in Section 4 which makes us compute the large-scale problem efficiently. In Section 5, several examples on computing the Casimir energy between the compact objects will be shown and we will also compare our results with others computed in other methods. Finally, Section 6 will conclude our paper and discuss the future plan as well.

2. Numerical methods for computing the Casimir energy in acoustic scattering

In this section, we are going to investigate the numerical methods on computing the Casimir energy. We would like to use the following notations for the domains of the boundary integral operators in both scalar and vector case. Assume $\Omega^- \in \mathbb{R}^d$, for $d \geq 2$ is the interior bounded Lebesgue-measurable domain that the scatterer occupies with Lipschitz-continuous boundary Γ and $\Gamma := \partial\Omega$ has a finite number of smooth faces that meet at non-degenerate edges and corners. In addition, the exterior domain is denoted as $\Omega^+ = \mathbb{R}^d\backslash\overline{\Omega^-}$. $\boldsymbol{n}$ is the exterior unit normal to the surface Γ pointing outwards from Ω^- and $\boldsymbol{n_x}$ is normal to Γ at the point $\boldsymbol{x} \in \Gamma$.

In the scalar case, the Casimir energy can be expressed in terms of the single-layer boundary operator and we will start from defining the function space on which the boundary operators are well-defined and Dirichlet trace operator, then give the definition of the single-layer boundary operator. Afterwards, the relation between the Krein spectral shift function with this operator will be introduced and finally, the numerical framework for computing the Casimir energy in the scalar case via the Galerkin discretization of the single-layer boundary operator.

2.1. Scalar function space and trace operator

For the bounded interior domain $\Omega^{\pm}$ or the unbounded exterior domain Ω^{+}, the space of the square integrable functions is

$$L^2(\Omega^{\pm}) := \left\{ f : \Omega^{\pm} \to \mathbb{C}, f \text{ is Lebesgue measurable and } \int_{\Omega^{\pm}} |f|^2 < \infty \right\}$$

and the Sobolev space $H^s(\Omega^{\pm})$ is defined as

$$H^s(\Omega^{\pm}) := \left\{ f \in L^2(\Omega^{\pm}), \forall \alpha \text{ s.t.} |\alpha| \le s, D^{\alpha} f \in L^2(\Omega^{\pm}) \right\},$$

where $\alpha = (\alpha_1, \alpha_2, \ldots, \alpha_d)$ is a multi-index and $|\alpha| = \alpha_1 + \alpha_2 + \cdots + \alpha_d$, and the derivative is defined in the weak sense.

To construct the single-layer boundary operator, we also need the Dirichlet trace operator $\gamma_{\mathrm{D}}^{\pm} : H^1(\Omega^{\pm}) \to H^{\frac{1}{2}}(\Gamma)$: for sufficiently smooth function p,

$$\gamma_{\mathrm{D}}^{\pm} p(\boldsymbol{x}) := \lim_{\Omega^{\pm} \ni \boldsymbol{x}' \to \boldsymbol{x} \in \Gamma} p(\boldsymbol{x}'),$$

where the subscripts $^-$ and $^+$ denote the interior and exterior traces, respectively.

2.2. Single-layer boundary integral operator

Typically, the *single-layer potential operator* $\mathcal{V}_k : H^{-\frac{1}{2}}(\Gamma) \to H^1(\Omega^{\pm})$ can be represented as

$$(\mathcal{V}_k \mu)(\boldsymbol{x}) := \int_{\Gamma} g_k(\boldsymbol{x}, \boldsymbol{y}) \psi(\boldsymbol{y}) dS_{\boldsymbol{y}}, \qquad \text{for } \mu \in H^{-\frac{1}{2}}(\Gamma) \text{ and } \boldsymbol{x} \in \Omega^{\pm} \backslash \Gamma,$$

where $g_k(\boldsymbol{x}, \boldsymbol{y})$ is the fundamental solution of the Helmholtz operator and especially,

$$g_k(\boldsymbol{x}, \boldsymbol{y}) = \begin{cases} \frac{\mathrm{i}}{4} H_0^{(1)}(k|\boldsymbol{x} - \boldsymbol{y}|), & \text{for } d = 2 \\ \frac{e^{ik|\boldsymbol{x}-\boldsymbol{y}|}}{4\pi|\boldsymbol{x}-\boldsymbol{y}|}, & \text{for } d = 3, \end{cases}$$

where $H_0^{(1)}$ is a Hankel function of the first kind.

Now we can derive the *single-layer boundary operator* $V_k : H^{-\frac{1}{2}}(\Gamma) \to H^{\frac{1}{2}}(\Gamma)$ from this potential operator:

$$(V_k \mu)(\boldsymbol{x}) := \{\gamma_{\mathrm{D}} \mathcal{V}_k \mu\}_{\Gamma}(\boldsymbol{x}).$$

Combining with the jump condition

$$[\gamma_{\mathrm{D}}]_{\Gamma} \mathcal{V}_k = \gamma_{\mathrm{D}}^+ \mathcal{V}_k - \gamma_{\mathrm{D}}^+ \mathcal{V}_k = 0,$$

we can derive that

$$\gamma_{\mathrm{D}}^+ \mathcal{V}_k = \gamma_{\mathrm{D}}^- \mathcal{V}_k = V_k,$$

for the exterior and interior traces and the single-layer boundary operator writes

$$(V_k \mu)(\boldsymbol{x}) := \int_{\Gamma} g_k(\boldsymbol{x}, \boldsymbol{y}) \psi(\boldsymbol{y}) dS_{\boldsymbol{y}}, \qquad \text{for } \mu \in H^{-\frac{1}{2}}(\Gamma) \text{ and } \boldsymbol{x} \in \Gamma.$$

2.3. Relation between the Krein spectral shift function and the single-layer boundary operator

By [11], the Krein spectral shift function is defined as

$$\xi(k) = \frac{1}{2\pi \mathrm{i}} \log \left(\frac{\det(S(k))}{\det(S_{1,k}) \cdots \det(S_{N,k})} \right),$$

where $S_{i,n}$ is the scattering matrix associated with the nth scatterer. These scattering matrices can be constructed $S_{i,n} = I + T_{i,n}$, where I is the identity matrix and $T_{i,n}$ is the T-matrix and the method of computing the T-matrix is fully discussed in [12] and [13].

The following theorem links the single-layer boundary operator with the Krein spectral shift function which inspires us to computing the Casimir energy via the scattering matrix or integral operator.

Theorem 1. *[11] Consider Ω as a domain assembling from individual objects Ω_i. Let V_k be the single-layer boundary operator defined on the boundary $\partial\Omega = \bigcup_{i=1}^{N} \partial\Omega_i$, and $\tilde{V}_k^{-1}$ is the 'diagonal part' of V_k by restricting the integral kernel to the subset $\bigcup_{i=1}^{N} \partial\Omega_i \times \partial\Omega_i \subset \partial\Omega \times \partial\Omega$ then the operator $V_k \tilde{V}_k^{-1}$ is trace-class and*

$$\Xi(k) = \log \det \left(V_k \tilde{V}_k^{-1} \right).$$

Then for $k > 0$, we have

$$-\frac{1}{\pi} \mathrm{Im}\Xi(k) = \frac{\mathrm{i}}{2\pi} (\Xi(k) - \Xi(-k)) = \xi(k)$$

and by choosing $f(x) = x$ in (4), this gives the formula

$$\mathrm{Tr} \left(\Delta^{\frac{1}{2}} + (N-1)\Delta_0^{\frac{1}{2}} - \sum_{i=1}^{N} \Delta_j^{\frac{1}{2}} \right) = \int_0^\infty \xi(k)dk = -\frac{1}{\pi} \int_0^\infty \Xi(\mathrm{i}k)dk. \tag{5}$$

The equation (5) is used to compute the Casimir energy between the objects and the formula is written as

$$\mathcal{E} = \frac{\hbar c}{2} \int_0^\infty \xi(k)dk = -\frac{\hbar c}{2\pi} \int_0^\infty \Xi(\mathrm{i}k)dk \tag{6}$$

Remark 1. *Note that the integral $\frac{\hbar c}{2} \int_0^\infty \xi(k)dk$ in (6) is not Lebesgue integrable. Therefore, if one wants to compute the Casimir energy via the scattering matrix method, we should take use of the Gaussian exponential to help us compute this integral, which looks like:*

$$\frac{\hbar c}{2} \int_0^\infty \xi(k)dk = \lim_{t \to 0} \frac{\hbar c}{2} \int_0^\infty e^{-tk^2} \xi(k)dk. \tag{7}$$

The method of evaluating this integral is to firstly evaluate the function $\xi(k)$ in several interpolation points and then compute the numerical integral for various values of t and make t tend to zero.

2.4. Galerkin discretization and boundary element spaces

In order to compute the integral (6), we need to compute the log determinant of the operators $V_k \tilde{V}_k^{-1}$. In our numerical framework, we would like to use the Galerkin discretization to express the operators in matrix form and in this part, the explicit form of the element inside the matrix will be given and the Corresponding basis functions will be introduced as well.

Recall the domain of the single-layer boundary operator is $H^{-\frac{1}{2}}(\Gamma)$. To discretize this Sobolev space, we would lke to introduce the triangulation $\mathcal{T}_h$ of the boundary surface Γ with triangular surface elements τ_l and associated nodes $\boldsymbol{x}_i$ s.t. $\overline{\mathcal{T}_h} = \bigcup_l \overline{\tau_l}$, where h is the mesh size and define the space of the continuous piecewise linear functions

$$P_h^1(\Gamma) = \{v_h \in C^0(\Gamma) : v_h|_{\tau_l} \in \mathbb{P}_1(\tau_l), \text{ for } \tau_l \in \mathcal{T}_h\},$$

where $\mathbb{P}_1(\tau_l)$ denotes the space of polynomials of order less than or equal to 1 on τ_1 and typically, we use the following $P_h^1(\Gamma)$ space to discretize $H^{-\frac{1}{2}}(\Gamma)$:

$$P_h^1(\Gamma) := \operatorname{span}\{\phi_j\} \subset H^{-\frac{1}{2}}(\Gamma)$$

with

$$\phi_j(\boldsymbol{x}_j) = \begin{cases} 1, & i = j, \\ 0, & i \neq j. \end{cases}$$

Having defined the basis function $P_h^1(\Gamma)$, we can represent each element inside the Galerkin discretization form. Assume there are N objects, then the matrix of the operator V_k is an N by N block matrix, written as

$$\mathsf{V}_k = \mathsf{V}(k) = \begin{bmatrix} \mathsf{V}_{11}(k) & \mathsf{V}_{12}(k) & \cdots & \mathsf{V}_{1N}(k) \\ \mathsf{V}_{21}(k) & \mathsf{V}_{22}(k) & \cdots & \mathsf{V}_{2N}(k) \\ \vdots & \vdots & \ddots & \vdots \\ \mathsf{V}_{N1}(k) & \mathsf{V}_{N2}(k) & \cdots & \mathsf{V}_{NN}(k) \end{bmatrix}$$

and the matrix $\tilde{V}_k$ is the diagonal part of V_k:

$$\tilde{\mathsf{V}}_k = \tilde{\mathsf{V}}(k) = \begin{bmatrix} \mathsf{V}_{11}(k) & 0 & \cdots & 0 \\ 0 & \mathsf{V}_{22}(k) & \cdots & 0 \\ \vdots & \vdots & \ddots & \vdots \\ 0 & 0 & \cdots & \mathsf{V}_{NN}(k) \end{bmatrix}.$$

Therefore, the element in the mth row and nth column of the block matrix $\mathsf{V}_{ij}(k)$ is

$$\mathsf{V}_{ij}^{(m,n)}(k) = \langle V_{ij}(k)\phi_m^i, \phi_n^j \rangle = \int_\Gamma \overline{\phi_n^{(j)}}(\boldsymbol{x}) \int_\Gamma g_k(\boldsymbol{x}, \boldsymbol{y})\phi_m^{(i)}(\boldsymbol{y}) dS_{\boldsymbol{y}} dS_{\boldsymbol{x}}, \tag{8}$$

where $\boldsymbol{\phi}^i = \begin{bmatrix} \phi_1^{(i)} & \phi_2^{(i)} & \cdots & \phi_N^{(i)} \end{bmatrix}$ is the set of basis functions defined on the ith object and

$$\langle f, g \rangle = \int_\Gamma \overline{f(\boldsymbol{x})} g(\boldsymbol{x}) dS_x$$

denotes the standard $L^2(\Gamma)$ inner product.

By (8), the explicit form of each element in matrix V and $\tilde{\mathsf{V}}_k$ is known, therefore, the value of $\Xi(ik) = \log \det(V_{ik}\tilde{V}_{ik}^{-1})$ can be evaluated by computing $\log \frac{\det \mathsf{V}_{ik}}{\det \tilde{\mathsf{V}}_{ik}}$ with different values of k, which is the integrand of the Casimir formula (6). However, by plotting the value of this integrand with respect to different values of ik, we found that this function is exponentially decays with increasing the imaginary wavenumber ik (see Figure 1) and with this property, we suggest using the normal trapezoidal rule to calculate the integral $\int_0^\infty \Xi(ik)dk = \int_0^\infty \log \frac{\det \mathsf{V}_{ik}}{\det \tilde{V}_{ik}} dk$. The steps are sketched as follows.

- Set $f(k) = \log \frac{\det \mathsf{V}_{ik}}{\det \tilde{V}_{ik}}$ and the range of k is from 0 to ∞.

- Let $k = -\log(y)$, then the integral $\int_0^\infty \log \frac{\det \mathsf{V}_{ik}}{\det \tilde{V}_{ik}} dk$ becomes $\int_0^\infty f(k)dk = \int_0^1 \frac{f(-log(y))}{y} dy$.

- Set the range of k as (lb, ub) [1] and the corresponding range for y is $(e^{-ub}, e^{-lb}) \subset [0, 1]$.

- Choose m quadrature points from the interval (e^{-ub}, e^{-lb}) and use the trapezoidal rule to evaluate the integral $\int_{e^{-ub}}^{e^{-lb}} \frac{f(-log(y))}{y} dy$. Figure 2 plots the integrand with regard to new variable $y(= e^{-k})$.

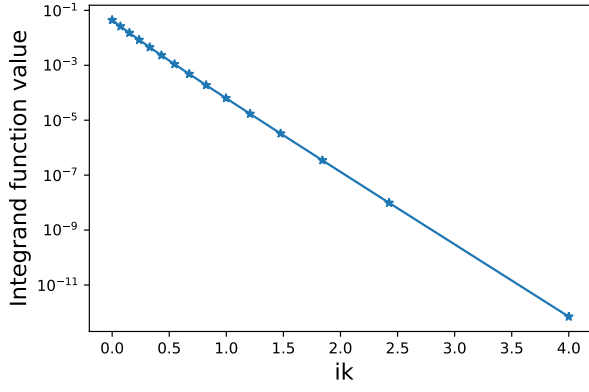[1] "ub" is short for upperbound and "lb" is short for lowerbound.

Figure 1: The integrand of the Casimir energy whose value exponentially decays with increasing imaginary wavenumber ik.
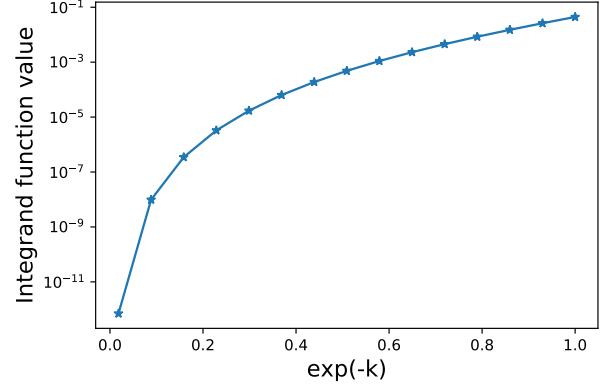

Figure 2: The integrand of the Casimir energy after changing the variable for applying the trapezoid quadrature rule.

3. Spectral property of the integral operators

The matrix M_∞ is a compact perturbation of matrix M, which makes the eigenvalues of them close to each other. Therefore, if we plot the eigenvalues of the matrix MM_∞^{-1}, we can notice that there are many eigenvalues closed to 1 and nearly contributes nothing to the log determinant. This spectral property inspires us to use some iteration method to approximate the extreme eigenvalues of MM_∞^{-1}. In order to make the computation process more efficiently, we will introduce an inverse-free method to speed up this process which makes us deal with the large-scale problem in the future.

4. Inverse-free methods for computing $\log\det(\mathsf{V}_{\mathrm{i}k}\tilde{\mathsf{V}}_{\mathrm{i}k}^{-1})$

By Section 2, to compute the Casimir energy, we need to evaluate $\log\frac{\det\mathsf{V}_{\mathrm{i}k}}{\det\tilde{\mathsf{V}}_{\mathrm{i}k}} = \log\det(\mathsf{V}_{\mathrm{i}k}\tilde{\mathsf{V}}_{\mathrm{i}k}^{-1})$ with different values of k. In this section, an efficient inverse-free method will be introduced to compute this log determinant.

The log determinant of the matrix $\mathsf{V}_{\mathrm{i}k}\tilde{\mathsf{V}}_{\mathrm{i}k}^{-1}$ is equal to the sum of the logarithm of each eigenvalue of $\mathsf{V}_{\mathrm{i}k}\tilde{\mathsf{V}}_{\mathrm{i}k}^{-1}$. From Figure 3, we can notice that most of the eigenvalues are just equal to 1, which contributes nothing on the value of Casimir energy. Therefore, the computation process for the large-scale problem can become efficient if we only approximate the extreme eigenvalues which mainly contribute to the log determinant. In addition, we should also avoid directly computing the inverse of the matrix $\tilde{\mathsf{V}}_{\mathrm{i}k}$ since the computational complexity is cubic with respect to the matrix dimension.

In what follows, an inverse-free Krylov subspace method will be introduced to computed multiple smallest (or largest) eigenvalues of the generalized eigenvalue problems simultaneously. Afterwards, we will discuss another inverse-free method based on LU decomposition of the diagonal block matrix of $\tilde{\mathsf{V}}_{\mathrm{i}k}$. Finally, the comparison of these two methods will be shown.
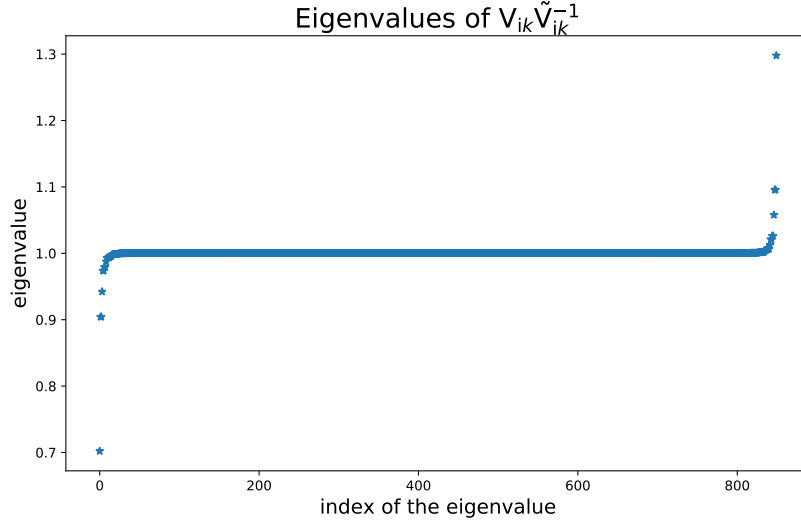
Figure 3: The eigenvalues of the matrix $\mathsf{V}_{ik}\tilde{\mathsf{V}}_{ik}^{-1}$ when $ik = 0.8i$.

4.1. Method I: Krylov subspace for generalized eigenvalue problem

Consider the eigenvalue problem:

$$\mathsf{V}_{ik}\tilde{\mathsf{V}}_{ik}^{-1}\boldsymbol{x} = \lambda\boldsymbol{x}, \tag{9}$$

where λ is the eigenvalue and $\boldsymbol{x}$ is the corresponding eigenvalue. This eigenvalue problem is equivalent to the following generalized eigenvalue problem:

$$\mathsf{V}_{ik}\tilde{\boldsymbol{x}} = \lambda\tilde{\mathsf{V}}_{ik}\tilde{\boldsymbol{x}}. \tag{10}$$

Thus, we can focus on solving the problem (10) instead of (9) to avoid computing the matrix inversion. By [14], the authors proposed an inverse-free Krylov subspace method for computing multiple eigenvalues of the symmetric definite generalized eigenvalue problem simultaneously and the following algorithm summarizes this method.

Algorithm 1: Inverse-free Krylov subspace method for computing p smallest eigenvalues of the generalized eigenvalue problem $A\boldsymbol{x} = \lambda B\boldsymbol{x}$

Input: Symmetric matrix $A \in \mathbb{R}^{n \times n}$, s.p.d matrix $B \in \mathbb{R}^{n \times n}$ and a B-orthonormal matrix $X^{(1)} \in \mathbb{R}^{n \times p}$ with $X^{(1)*}BX = I_p$ and $m \geq 1$

Output: The approximated p smallest eigenvalues of $A\boldsymbol{x} = \lambda B\boldsymbol{x}$

  1: Set $\Theta^{(1)} = \text{diag}(X^{(1)*}AX^{(1)})$

  2: **for** $k = 1, 2, \ldots$ **do**

  3:   **for** $i = 1, 2, \ldots, p$ **do**

  4:     Construct a basis $\hat{Z}_i$ of the ith Krylov subspace $K_m(A - \theta_i^{(k)}B, x_i^{(k)})$ with dimension m

  5:     Orthonormalize $\left[\hat{Z}_1 \cdots \hat{Z}_p\right]$ to obtain Z

  6:     Project A and B on Z: $A_m = Z^*AZ$, $B_m = Z^*BZ$

  7:     Compute p smallest eigenpairs (θ_i, u_i), $1 \leq i \leq p$ of the matrix pencil (A_m, B_m)

  8:     $\Theta^{(k+1)} = \text{diag}(\theta_1, \ldots, \theta_p)$; $X^{(k+1)} = ZU$, $U = (u_1 \cdots u_p)$

  9:   **end for**

  10: **end for**

Algorithm 1 can make us approximate p smallest eigenvalues of the matrix pencil (A, B) and the most trivial way to compute the p largest eigenvalues is to use the same algorithm as above but only change the matrix M to $-M$. Then we can find the p smallest eigenvalues of $(-A, B)$ and by adding the negative sign in front of these eigenvalues, we can obtain p largest eigenvalues of (A, B).

We denote the p smallest (or largest) eigenvalues obtained from this method as

$$\Lambda_{\text{Kry}}^{\text{smallest}} = \left\{ \lambda_0^{(s)}, \lambda_1^{(s)}, \ldots, \lambda_{p-1}^{(s)} \right\}, \tag{11}$$

$$\Lambda_{\text{Kry}}^{\text{largest}} = \left\{ \lambda_0^{(l)}, \lambda_1^{(l)}, \ldots, \lambda_{p-1}^{(l)} \right\}. \tag{12}$$

Then, the value of $\log \det(\mathsf{V}_{ik} \tilde{\mathsf{V}}_{ik}^{-1})$ can be approximated by

$$\log \det(\mathsf{V}_{ik} \tilde{\mathsf{V}}_{ik}^{-1}) \approx \sum_{i=0}^{p} \log \left(\lambda_i^{(s)} \right) + \sum_{i=0}^{p} \log \left(\lambda_i^{(l)} \right)$$

4.2. Method II: LU decomposition for inverting the matrix

Another inverse-free way to compute $\log \det(\mathsf{V}_{ik} \tilde{\mathsf{V}}_{ik}^{-1})$ is to find the *LU* decomposition of each diagonal block matrix and solve the linear system on each subdomain. To be specific, the inverse of the matrix $\tilde{\mathsf{V}}_{ik}$ is

$$\tilde{\mathsf{V}}_{ik}^{-1} = \tilde{\mathsf{V}}(ik)^{-1} = \begin{bmatrix} \mathsf{V}_{11}(ik) & 0 & \cdots & 0 \\ 0 & \mathsf{V}_{22}(ik) & \cdots & 0 \\ \vdots & \vdots & \ddots & \vdots \\ 0 & 0 & \cdots & \mathsf{V}_{NN}(ik) \end{bmatrix}^{-1} = \begin{bmatrix} \mathsf{V}_{11}^{-1}(ik) & 0 & \cdots & 0 \\ 0 & \mathsf{V}_{22}^{-1}(ik) & \cdots & 0 \\ \vdots & \vdots & \ddots & \vdots \\ 0 & 0 & \cdots & \mathsf{V}_{NN}^{-1}(ik) \end{bmatrix}$$

We can compute *LU* decomposition of each diagonal block matrix $\mathsf{V}_{ii} = \mathsf{V}_{ii}(ik)$ for $i = 1, 2, \ldots, N$ and the decomposition is written as $\mathsf{V}_{ii} = \mathsf{L}_{ii} \mathsf{U}_{ii}$, where L_{ii} is a lower triangular matrix and U_{ii} is upper triangular. Afterwards, we solve the linear system $\mathsf{L}_{ii} \mathsf{U}_{ii} \boldsymbol{x_j} = \boldsymbol{e}_j$, for $j = 1, 2, \ldots, N_{\mathsf{V}_{ii}}$, where $\boldsymbol{e}_j$ denotes the vector with a 1 in the jth coordinate and 0's elsewhere and $N_{\mathsf{V}_{ii}}$ is the dimension of the block V_{ii}. Finally, the inverse of V_{ii} is $\mathsf{V}_{ii}^{-1} = \begin{bmatrix} \boldsymbol{x}_1 & \cdots & \boldsymbol{x}_{N_{\mathsf{V}_{ii}}} \end{bmatrix}$ and we can notice that this whole process contains no step that needs us to compute the inverse of any matrix.

We denote the inverse of the matrix $\tilde{\mathsf{V}}_{ik}$ computed by the above inverse-free *LU* decomposition method as $\tilde{\mathsf{V}}_{ik}^{-1,\text{LU}}$ and to approximate multiple extreme eigenvalues of $\mathsf{V}_{ik} \tilde{\mathsf{V}}_{ik}^{-1,\text{LU}}$, we would like to firstly construct the Krylov subspace $K_m(\mathsf{V}_{ik} \tilde{\mathsf{V}}_{ik}^{-1,\text{LU}}, \boldsymbol{b})$, where $\boldsymbol{b}$ is some initial vector and m is the dimension of this subspace. Afterwards, we implement the Arnold iteration to obtain the orthogonal basis of this mth Krylov subspace and project the matrix $\mathsf{V}_{ik} \tilde{\mathsf{V}}_{ik}^{-1,\text{LU}}$ onto this basis. This projection matrix is called the Hessenberg matrix and we denote it as H_m. By [15], the eigenvalues of H_m (which are also called Ritz eigenvalues) can give good approximations to some eigenvalues of $\mathsf{V}_{ik} \tilde{\mathsf{V}}_{ik}^{-1,\text{LU}}$. Therefore, we denote the the eigenvalues of H_m as

$$\Lambda_{\text{Hess}} = \left\{ \lambda_0^{(\text{Hess})}, \lambda_1^{(\text{Hess})}, \ldots, \lambda_{m-1}^{(\text{Hess})} \right\} \tag{13}$$

and the value of $\log \det(\mathsf{V}_{ik} \tilde{\mathsf{V}}_{ik}^{-1})$ can be approximated by

$$\log \det(\mathsf{V}_{ik} \tilde{\mathsf{V}}_{ik}^{-1}) \approx \sum_{i=0}^{m-1} \log \left(\lambda_i^{(\text{Hess})} \right).$$

4.3. Comparison of two inverse-free methods

Figure 4 plots multiple smallest and largest approximated eigenvalues of the matrix $\mathsf{V}_{ik} \tilde{\mathsf{V}}_{ik}^{-1}$ when $p = 25$ (for p in Method I) and the dimension of the Krylov subspace in both line four of Algorithm 1 and Method II is $m = 50$.
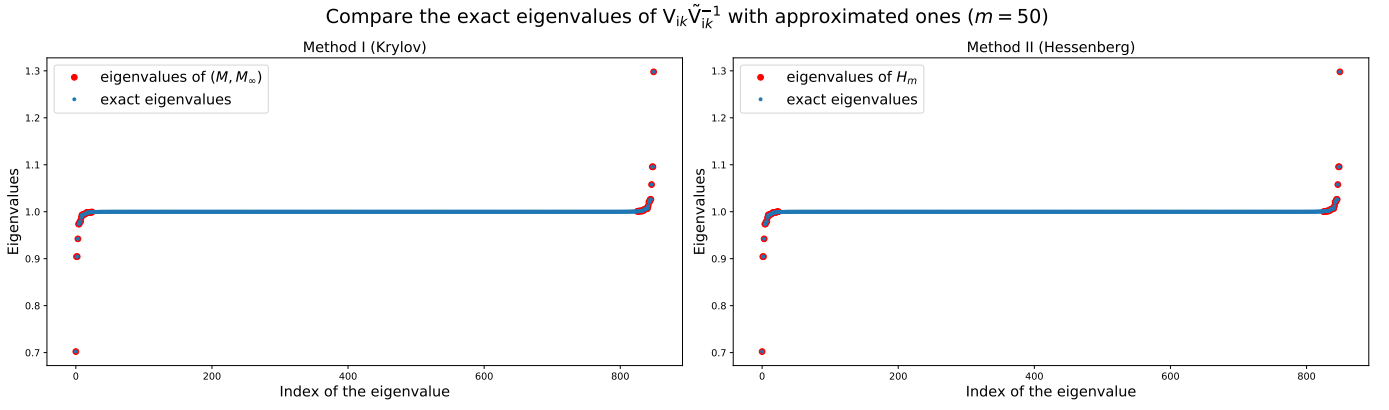
Figure 4: Comparison between p approximated smallest eigenvalues and p largest ones with the exact eigenvalues when $p = 25$ and the dimension of the Krylov subspace in both line four of Algorithm 1 and Method II is set as $m = 50$.

By Figure 4, the approximated extreme eigenvalues are quite close to the exact ones and in order to see how close they are, we plot the relative error between them in Figure 5.
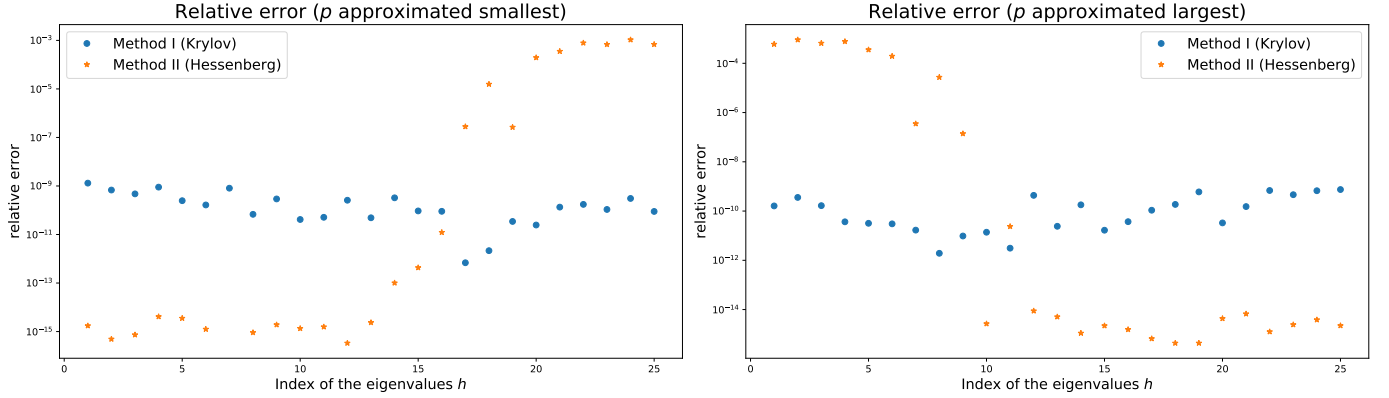

Figure 5: (Left) The relative error of the p ($p = 25$) smallest eigenvalues between the exact and approximated ones. (Right) The relative error of the p ($p = 25$) largest eigenvalues between the exact and approximated ones.

To more intuitively see which inverse-free method is better, we would like to fix the dimension of the Krylov subspace as $m = 50$ and increase the number of the approximated eigenvalues from 2 to 50 and then plot the relative error in each case. The procedure is as follows.

For example, when the number of the approximated eigenvalue is 2, the relative error for the Method I (Krylov) is computed by:

$$\text{Err}_{\text{Kry}}^{(2)} = \frac{\left(\log(\lambda_0^{(s)}) + \log(\lambda_{p-1}^{(l)})\right) - \text{exact\_logdet}}{\text{exact\_logdet}},$$

where exact_logdet is the exact value of the log determinant of $\mathsf{V}_{ik}\tilde{\mathsf{V}}_{ik}^{-1}$ and $\lambda_0^{(s)}$, $\lambda_{p-1}^{(l)}$ are from the sorted sets $\Lambda_{\text{Kry}}^{\text{smallest}}$ in (11) and $\Lambda_{\text{Kry}}^{\text{largest}}$ in (12), respectively; and the relative error for the Method II (Hessenberg) is computed by

$$\text{Err}_{\text{Hess}}^{(2)} = \frac{\left(\log(\lambda_0^{\text{Hess}}) + \log(\lambda_{m-1}^{\text{Hess}})\right) - \text{exact\_logdet}}{\text{exact\_logdet}},$$

where λ_0^{Hess} and $\lambda_{m-1}^{\text{Hess}}$ are both from the sorted set Λ_{Hess} in (13).

The following graph plots the relative error computed in both cases and we can see that their relative errors shares the same trend at the beginning and the Method II (Hessenberg) becomes worse when the number of the approximated eigenvalues becomes close to the dimension of the Krylov subspace.
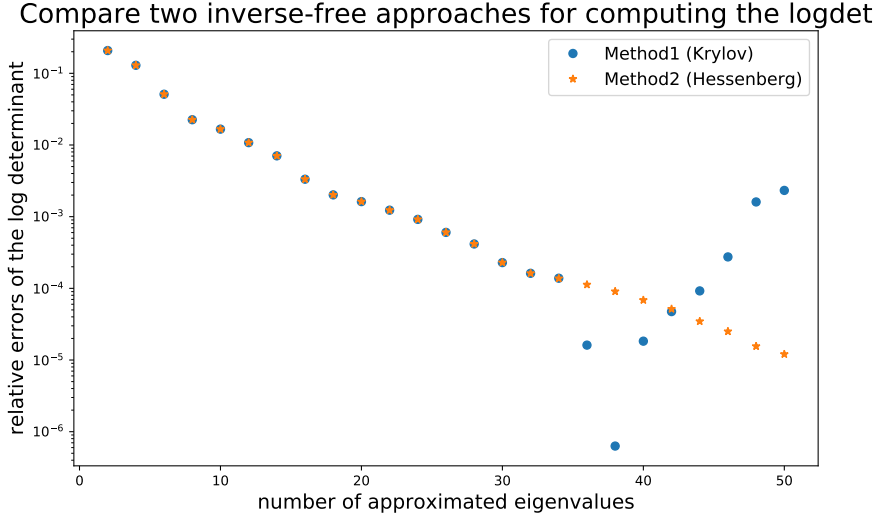
Figure 6: The comparison between two inverse-free methods by fixing the dimension of the Krylov subspace as $m = 50$ and increasing the number of the approximated eigenvalues from 2 to 50.

5. Numerical experiments

5.1. Two-spheres case

The scatterers are two spheres and we compute the Casimir energy between them with the centering distance $Z = 2.5, 3.5, 5$ in the scalar and vector case; we also have the asymptotic series in the scalar and vector cases. Finally, we compare the results obtained from different methods.

5.2. Realistic objects case

The scatterers are set as some realistic objects (or something complex such as 8-branch ice crystal) and we compute the Casimir energy between them in the scalar and vector case. Finally, we compare the results obtained from different methods.

6. Conclusion

.

References

References

[1] H. B. Casimir, On the attraction between two perfectly conducting plates, in: Proc. Kon. Ned. Akad. Wet., Vol. 51, 1948, p. 793.

[2] I. E. Dzyaloshinskii, E. M. Lifshitz, L. P. Pitaevskii, The general theory of van der waals forces, Advances in Physics 10 (38) (1961) 165–209.

[3] S. K. Lamoreaux, Demonstration of the casimir force in the 0.6 to 6 μ m range, Physical Review Letters 78 (1) (1997) 5.

[4] T. Ederth, Template-stripped gold surfaces with 0.4-nm rms roughness suitable for force measurements: Application to the casimir force in the 20–100-nm range, Physical Review A 62 (6) (2000) 062104.

[5] G. Bressi, G. Carugno, R. Onofrio, G. Ruoso, Measurement of the casimir force between parallel metallic surfaces, Physical review letters 88 (4) (2002) 041804.

[6] D. Krause, R. Decca, D. López, E. Fischbach, Experimental investigation of the casimir force beyond the proximity-force approximation, Physical review letters 98 (5) (2007) 050403.

[7] H. B. Chan, Y. Bao, J. Zou, R. Cirelli, F. Klemens, W. Mansfield, C. Pai, Measurement of the casimir force between a gold sphere and a silicon surface with nanoscale trench arrays, Physical review letters 101 (3) (2008) 030401.

[8] T. Emig, N. Graham, R. Jaffe, M. Kardar, Casimir forces between compact objects: The scalar case, Physical Review D 77 (2) (2008) 025005.

[9] T. Emig, N. Graham, R. Jaffe, M. Kardar, Casimir forces between arbitrary compact objects, Physical review letters 99 (17) (2007) 170403.

[10] M. H. Reid, A. W. Rodriguez, J. White, S. G. Johnson, Efficient computation of casimir interactions between arbitrary 3d objects, Physical review letters 103 (4) (2009) 040401.

[11] F. Hanisch, A. Strohmaier, A. Waters, A relative trace formula for obstacle scattering, arXiv preprint arXiv:2002.07291 (2020).

[12] P. Waterman, New formulation of acoustic scattering, The journal of the acoustical society of America 45 (6) (1969) 1417–1429.

[13] M. Ganesh, S. C. Hawkins, A far field based t-matrix method for three dimensional acoustic scattering, ANZIAM Journal 50 (2008) 121–136.

[14] P. Quillen, Q. Ye, A block inverse-free preconditioned krylov subspace method for symmetric generalized eigenvalue problems, Journal of computational and applied mathematics 233 (5) (2010) 1298–1313.

[15] Y. Saad, Numerical methods for large eigenvalue problems: revised edition, SIAM, 2011.